Shot noise suppression at one-dimensional hopping

Alexander N. Korotkov and Konstantin K. Likharev
Department of Physics and Astronomy, State University of New York, Stony Brook, New York 11794-3800
(Received 15 December 1999)

We have carried out a preliminary analysis of shot noise at hopping, focusing on uniform one-dimensional (1D) arrays of sites separated by N tunnel barriers. The results show that at low temperatures the low-frequency density of the shot noise varies from $1/N$ to 1 of the Schottky value, depending on the geometry, electron density, and Coulomb interaction strength. An interesting feature is $\omega^{-1/3}$ dependence of the current spectral density at intermediate frequencies, which reflects self-similarity of the fluctuations at different size scales.

I. INTRODUCTION

Nonequilibrium fluctuations in mesoscopic systems can present additional information that is not reflected in their dc transport characteristics. This is one of the reasons why ''shot noise'' (i.e., nonequilibrium fluctuations of current with constant or nearly constant spectral density at low frequencies) has attracted so much attention in mesoscopics during the last decade—see, e.g., Refs. 1–3.

An additional motivation for the present paper was provided by the observation[4] that the smallness of the shot noise is a necessary condition for quasicontinuous electron transfer. More exactly, for an external observer a conductor provides effectively Ohmic (quasi-continuous) conduction only if the so-called Fano factor

$$F \equiv S_I(0)/2e\langle I\rangle \tag{1}$$

(where $S_I(0)$ is the low-frequency density of current fluctuations, and $\langle I\rangle$ is the average current) is much lower than 1. If simultaneously the resistance of such a sample is sufficiently high, and its stray capacitance is low,

$$R \gg \hbar/e^2, \quad C \ll e^2/T, \tag{2}$$

it may be used for resistive coupling in single-electron devices. Since using resistively coupled devices is one of the very few options available to avoid the forbidding problem of random background charge in single-electronics (see, e.g., Refs. 5,6), the search for systems with quasi-continuous conduction is important for possible future applications of single-electron devices in integrated circuits.

Shot noise has been extensively analyzed for metallic conduction (in both ballistic[7–9] and diffusive[10–14] limits) and for single-electron tunneling.[15–18] Unfortunately, metallic conductors can satisfy the condition $F \ll 1$ only if they are much longer than the electron-phonon interaction length.[12,14] As a result Eqs. (2) can be practically met only at very low temperatures—see, e.g., experiment.[19] The same is true for single-electron circuits [like one-dimensional (1D) or two-dimensional (2D) arrays] with their relatively large islands.[5,6]

Much higher resistance R at small sample length (and hence small C) is typical for hopping conductors—see, e.g., Refs. 20,21. Naively, one might think that since the hopping transport is due to discrete single-electron tunneling events (''hops''), the shot noise should be close to the Schottky value [$S_I(0)=2e\langle I\rangle$, i.e., $F=1$]. However, this argument is obviously not true, since it could also be applied to a 1D series array of N tunnel junctions. A simple ''circuit'' theory[22,23] (see also Appendix) shows that for such an array the Fano factor can be very small:

$$F \sim 1/N \ll 1. \tag{3}$$

The physical reason for this fact is that the noise originating from each junction is strongly shunted by the junction resistance, which is much smaller than the total resistance of other junctions.

Thus, there is hope of having the shot noise at hopping suppressed well below the Schottky value as well. However, the real picture of hopping is complex, and the noise may be much higher than the simple estimate given above. For example, mutual correlation of the hopping events, exponentially broad distribution of their rates due to sample randomness, and the percolative character of transport paths in 2D and three-dimensional (3D) cases[20,21] may all be important factors. Until recently, the situation was virtually unexplored: the few publications on the theory of noise in hopping that we are aware of (see, e.g., Ref. 24 and references therein) concentrate on $1/f$ noise rather than on the broadband shot noise.[25] We are also unaware of any experimental studies of noise at hopping at frequencies high enough to avoid $1/f$ noise dominance.

The goal of this paper is to develop an initial picture of shot noise at hopping. We will focus on the 1D case, and assume uniformity of hopping conditions between all the sites. (A brief analysis of nonuniform systems and higher dimensions is given in the discussion, Sec. V.) In principle, 1D hopping may be implemented experimentally using a linear array of quantum dots between two external electrodes [Fig. 1(a)]. Besides this geometry, we will also consider a somewhat artificial model of hopping on a ring [Fig. 1(b)], at least because problems with periodic boundary conditions are traditional in theoretical studies of hopping. Besides that, since such models automatically conserve the total electron number, they may crudely mimic ''open'' models [Fig. 1(a)] with considerable Coulomb interaction without its explicit account.

Throughout our analysis we will assume that the electron states localized at each site are nondegenerate, so that each site may be occupied with just one electron, or none. This

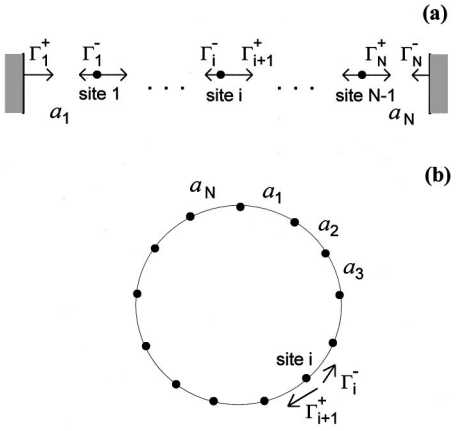

FIG. 1. (a) Linear array of $N-1$ localized sites connecting two electrodes (''open boundary conditions''). The electron transport is determined by the tunneling rates $\Gamma_i^{\pm}$. (b) Circular array (''periodic boundary conditions'') with N sites occupied by M electrons.

model can be viewed as a special case of the ''orthodox'' theory of single-electron tunneling[29] when the background charge of each island is close to $-e/2$, so that energies of two charge states ($n=0$ and $n=1$) are close to each other while other states are far beyond the available energy range. So, the well-developed theory of noise based either on Fokker-Planck[15–18] or Langevin[30] approach can be directly applied to any hopping structure with arbitrary electron-electron interaction. However, these approaches involve taking into account an exponentially large number of charge configurations, thus limiting practical calculations to relatively small structures, $N \lesssim 20$. This is why for the numerical results we have used the Monte Carlo approach, similar to that used for simulations of transport[31] and noise[16,4] at single-electron tunneling, with the corresponding restriction of the site state number.

It is instructive to compare the results for the shot noise at 1D hopping and at tunneling in 1D array of tunnel junctions. Some formulas necessary for this comparison are derived in the Appendix for the case of weak charge discreteness effects.

II. SOME GENERAL RELATIONS

In the hopping limit,[20,21] where quantum interference between states before and after each hopping event is neglected because of the inelastic nature of electron transport,[32] site occupation numbers may be considered as random classical variables. If we are not interested in extremely high frequencies (when the finite photon energy becomes important), current $I_i(t)$ flowing between the $(i-1)$th and ith site may be considered as a sum of infinitely short pulses:

$$I_i(t)=I_i^+(t)-I_i^-(t), \quad I_i^{\pm}(t)=\sum_{t_k} e\,\delta(t-t_k^{\pm}), \tag{4}$$

where t_k^+ (t_k^-) is the time of kth hop in the positive (negative) direction between the sites. In the ''open boundary'' problem [Fig. 1(a)], with a fixed voltage across the sample, we may also consider currents $I(t)$ flowing in external electrodes.[4,31] These currents contain contributions not only from the hops to and from the electrodes, but also the polarization charge changes (displacement current contribution) due to hops between internal sites:

$$I(t)=\sum_{i=1}^{N} \lambda_i I_i(t), \quad \sum_i \lambda_i = 1, \tag{5}$$

where the factors λ_i depend on the structure geometry and can be expressed via its electrostatic matrix—see Appendix. (In general, these coefficients are different for the left and right electrodes.) In the simplest case of a 1D array between two infinite parallel metallic plates, $\lambda_i = a_i/L$, $L \equiv \Sigma_i a_i$, where a_i is transport direction component of ith hop vector. In this work, we will use this formula, with $a_i = L/N = \text{const}$ (i.e., $\lambda_i = 1/N$), even for the ring geometry [Fig. 1(b)], though this model does not have any electrodes. This assumption is not critical for the Fano factor, which does not depend on λ_i, since at low frequencies the spectral densities of all currents I_i and I coincide. A simple proof of this statement may be obtained from the spectral density definition

$$S_I(\omega)=\lim_{\tau\to\infty}\frac{2}{\tau}\left\langle\left|\int_0^{\tau} I(t)e^{\imath\omega t}dt\right|^2\right\rangle \tag{6}$$

in the limit $\omega \to 0$, using the condition that the charge cannot accumulate indefinitely inside the array. In the opposite limit of high frequencies (much higher than the average tunneling rate, though still much lower than the reciprocal ''time of tunneling,'' which is considered infinitely short in our theory), the spectral densities of currents I_i and I are typically different, and obey a simple formula. In fact, in the high-frequency limit all tunnel events are effectively uncorrelated and the phases of factors $\exp(\imath\omega t_k^{\pm})$ in Eq. (6) are random. From this, we obtain

$$S_{I_i}(\infty)=2e(\langle I_i^+\rangle+\langle I_i^-\rangle), \quad S_I(\infty)=\sum_i \lambda_i^2 S_{I_i}(\infty). \tag{7}$$

It is easy to see that for the current through one barrier $S_{I_i}(\infty)/2e\langle I\rangle \geqslant 1$, while for the external current $S_I(\infty)/2e\langle I\rangle \geqslant 1/N$. We will mostly be interested in the readily measurable quantity $S_I(\omega)$ and its low-frequency value $S_I(0)$.

For the numerical (Monte Carlo) calculations of the spectral density we have directly used[16] Eq. (6). The time period τ is chosen to be sufficiently long and the averaging is done over many such time periods. In practical calculations, it is important to keep the product $\omega\tau/2\pi$ integer in order to avoid numerical inaccuracy at low frequencies, and it is convenient to calculate simultaneously the spectral density at several overtones of certain basic (low) frequency. For several figures we have also used the newly developed method for the calculation of spectral density, which gives much faster convergence; this method will be described elsewhere.

III. CIRCULAR ARRAY

A. The model

We start with the auxiliary problem of hopping of a fixed number (M) of electrons on a uniform ring of $N > M$ sites. The electron may hop to either of the neighboring sites, i.e., either clockwise (with a probability rate of Γ^+) or counter-

clockwise (with rate $\Gamma^- < \Gamma^+$), but only if the accepting site is empty. The rates $\Gamma^\pm$ should satisfy the Gibbs relation

$$\Gamma^-/\Gamma^+ = \exp(-W/T), \tag{8}$$

where W is the energy difference between the neighboring sites.[33] (Due to the circular geometry, a conceptually sound, though impractical, way to create this difference is to increase the magnetic flux through the ring area at a constant rate. However, we consider the circular array mostly as a simplification of the realistic linear array.)

For the comparison of the current noise with the Nyquist formula we will need the total resistance of the ring, which is naturally defined as

$$R_\Sigma = V/\langle I\rangle, \tag{9}$$

where the total ''voltage'' V is defined as NW/e (the dependence of the tunneling rate on W can be arbitrary).

In the final part of our analysis we will include the particle interaction following the unscreened Coulomb law, so that the potential energy of the system is

$$U\{\mathbf{r}_1,\mathbf{r}_2,\ldots,\mathbf{r}_M\} = e^2 \sum_{i<j} \frac{1}{|\mathbf{r}_i-\mathbf{r}_j|} = \frac{e^2}{a}\sum_{i<j}\frac{\pi}{N\sin\pi\dfrac{|n_i-n_j|}{N}}, \tag{10}$$

where n_i is the site occupied by the ith electron. The interaction is included into the model by adding the corresponding change of U at a hop to that ($\pm W$) describing the external field. Since in this case the tunneling rates are no longer constant, we will need to specify an explicit relation $\Gamma^\pm(W)$. In this case we will assume

$$\Gamma \equiv \Gamma^+ - \Gamma^- = W/eR_0, \tag{11}$$

where R_0 gives the scale of the effective resistance of a tunnel barrier between adjacent sites.

B. Single-particle limit

Let us assume $M=1$.[35] Then the current $I(t)$ consists of uncorrelated pulses, each transferring the charge $\pm e/N$, with rates Γ^+ and Γ^-, respectively. This is equivalent to the conventional case of one tunnel junction with the electron charge substituted by e/N, hence

$$\langle I\rangle = e(\Gamma^+ - \Gamma^-)/N, \tag{12}$$

and the spectral density is frequency independent,[1] $S_I(\omega) = S_I(0)$, with

$$S_I(0) = \frac{2e^2}{N^2}(\Gamma^+ + \Gamma^-) = 2e\langle I\rangle \frac{1}{N}\coth\frac{W}{2T}. \tag{13}$$

Figure 2 shows the corresponding Fano factor $F = N^{-1}\coth(W/2T)$, as a function of W. In thermodynamic equilibrium, $W=0$, the noise satisfies the Nyquist formula, $S_I = 4T/R_\Sigma$, which remains valid while $W \ll T$. At $W \to 0$ the Fano factor tends to infinity because the average current vanishes while the equilibrium thermodynamic fluctuations still produce a finite current noise. For $N \gg 1$ the Fano factor crosses unity at $W \simeq W_c = 2T/N \ll T$. Let us emphasize that since $W_c \ll T$, the noise at this crossover is still due to thermodynamically equilibrium fluctuations. Finally, if the applied field is high ($W \gg T$), the Fano factor is low:

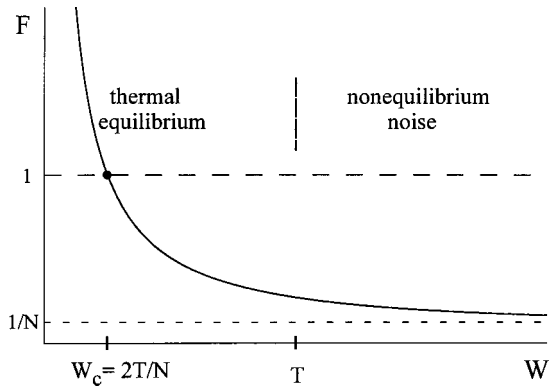

FIG. 2. The Fano factor F as a function of energy difference per site W in a circular array occupied by one electron.

$$F = 1/N. \tag{14}$$

Thus, as a matter of principle the shot noise suppression at hopping may be really very strong (proportional to the array length, just as in tunnel junction arrays). Now let us examine how this suppression is affected by various factors.

C. Low temperature, no interaction

At $T \ll W$ (i.e., $\Gamma \approx \Gamma^+ \gg \Gamma^-$) and in the absence of Coulomb interactions ($e^2/a \ll W$), but for arbitrary electron density $\rho \equiv M/N$ our model is reduced to the so-called asymmetric simple exclusion process (ASEP) model which has been extensively studied during the past few years–for a review see Ref. 26. Within this model, all $N!/M!(N-M)!$ possible charge configurations of the system have equal probability for the arbitrary N and M.[26] From this fact, the average current is readily calculated to equal

$$\langle I\rangle = e\Gamma\frac{M}{N}\frac{N-M}{N-1}, \tag{15}$$

so that for a large system ($N,M \to \infty$)

$$\langle I\rangle = e\Gamma\rho(1-\rho). \tag{16}$$

Notice that these expressions (as well as those below) are obviously symmetric over the transformation $\rho \leftrightarrow 1-\rho$, which interchanges electrons and holes. From Eq. (16), the maximum value $\langle I\rangle_{max} = e\Gamma/4$ of dc current is achieved at $\rho = 1/2$, which is a tradeoff between increasing concentration ρ and decreasing average velocity $\Gamma(1-\rho)$ of each electron (in hops per unit time) because of other electrons blocking its hops.

Equation (16) is exactly the result that could be anticipated in the complete absence of correlation between the hops. However, in fact these correlations *do* exist, as revealed, for example, by the spectral density of the current. Figure 3 shows the result of numerical calculation of $S_I(\omega)$ using the Monte Carlo approach for two concentrations, $\rho = 0.3$ and $\rho = 0.5$, and several values of the array length N.

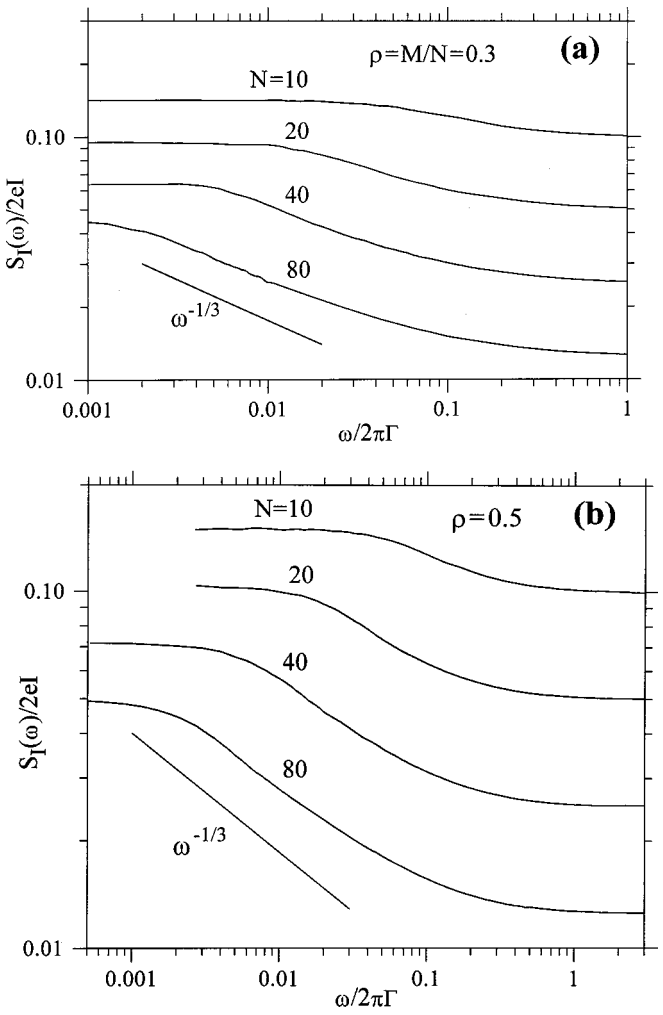

FIG. 3. Frequency dependence of the spectral density $S_I(\omega)$ for uniform circular arrays at $T=0$ for several values of array lengths N and electron concentration $\rho=M/N$: (a) $\rho=0.3$, (b) $\rho=0.5$.

The frequency dependence of the spectral density is obviously not flat as it would be in an uncorrelated case. With increasing N the spectral density decreases and forms three distinct regions as a function of frequency: low- and high-frequency saturation regions and almost power-law decay in between.

At high frequencies, in accordance with Eq. (7)

$$S_{I_i}(\infty)=2e\langle I\rangle, \quad S_I(\infty)=2e\langle I\rangle/N, \tag{17}$$

the suppression of the external current fluctuations is maximal. Notice that the frequency ω_h of the crossover to this limit apparently does not depend on N, while the low-frequency crossover occurs at frequency ω_l, which decreases with N crudely as $\omega_l \propto N^{-3/2}$. (In tunnel junction arrays, ω_l scales as N^{-2}–see Appendix). The zero-frequency limit has been studied analytically[26] giving the following Fano factor:

$$F=\frac{\pi^{1/2}}{2}\left[\frac{\rho(1-\rho)}{N}\right]^{1/2}, \quad \text{for } N,M\to\infty \tag{18}$$

(an analytical formula is also available[26] for arbitrary N and M). Figure 3 shows that at large N the frequency dependence of the current spectral density in the intermediate frequency range approaches the power law $S_I(\omega)\propto\omega^{-1/3}$.

This dependence may be interpreted as a consequence of the self-similarity of the fluctuations,[36] which occur at any site number scale L, within the interval $1\ll L\ll N$. In order to explain the $\omega^{-1/3}$ scaling, let us assume that Eq. (16) is applicable to long-wave density perturbations in our system and introduce two velocities (measured in sites per second) of their propagation.

The first of them, the sound (''shock''[26]) velocity

$$v_s=(1-2\rho)\Gamma, \tag{19}$$

can be found from the obvious continuity equation $\partial(e\rho)/\partial t=-\partial I/\partial x$, where I and ρ are understood in the sense of ''local'' averages over $1\ll\delta N\ll N$ sites and x is the site number considered as a continuous coordinate. Since these averages are related by Eq. (16), for small deviations from equilibrium we get $\partial\rho/\partial t=-(1-2\rho)\Gamma\partial\rho/\partial x$, i.e., an equation describing linear waves propagating with the speed given by Eq. (19). Notice that the sound velocity vanishes at half-filling, $\rho=1/2$, and is negative beyond this point.

In the circular array all density fluctuations move with the same sound velocity, so the fluctuation profile does not evolve in time and thus overall rotation does not affect the noise of current I (v_s will, however, be important later for the analysis of the linear array). To study the relaxation of density fluctuations we need to consider the deviations of v_s,

$$\delta v\simeq-\Gamma\,\delta\rho. \tag{20}$$

[Including the factor 2 following from Eq. (19) would be an overestimate of our accuracy, since such nonlinear velocity can be defined in various ways leading to different numerical coefficients.]

To calculate fluctuations $I(t)$ at a frequency $\omega\ll\Gamma$, we can integrate Eq. (16) over the whole circle taking into account local density fluctuations $\delta\rho$. Since we have assumed uniform λ_i in Eq. (5) and the total number of electrons does not fluctuate, $\int\rho(x)dx=M$, the contribution from the linear term $\delta I=e\Gamma(1-2\rho)\delta\rho$ vanishes. However, the current fluctuations do appear in the next, quadratic term of Eq. (16): $\delta I=-e\Gamma(\delta\rho)^2$, which describes the ''rectification'' of density fluctuations. [Somewhat paradoxically, this quadratic term does not affect the average current. This is because Eq. (16) is, strictly speaking, not valid for temporal dependence of current at finite size scale. Nevertheless, it can be applied to the analysis of fluctuations leading to the results which are correct up to a numerical factor.]

The density fluctuations at the size scale L ($1\ll L\ll N$) can be described by the binomial distribution, giving the variance $\langle(\delta\rho)^2\rangle=\rho(1-\rho)/L$. Hence, the typical relaxation bandwidth of these fluctuations (in the frame rotating with velocity v_s) is $\omega_L\simeq|\delta v|/L\simeq\Gamma[\rho(1-\rho)]^{1/2}L^{-3/2}$, and the corresponding spectral density is $S_\rho(\omega_L)\simeq(\delta\rho)^2/\omega_L\simeq[\rho(1-\rho)L]^{1/2}/\Gamma$. According to the standard theory of noise rectification (see, e.g., Ref. 37), $S_I(\omega_L)$ can be estimated as $(N/L)e^2\Gamma^2[S_\rho(\omega_L)]^2\omega_L$, where the first factor accounts for N/L virtually independent fluctuating regions. Combining these estimates and eliminating L (as a function of ω_L), we finally obtain

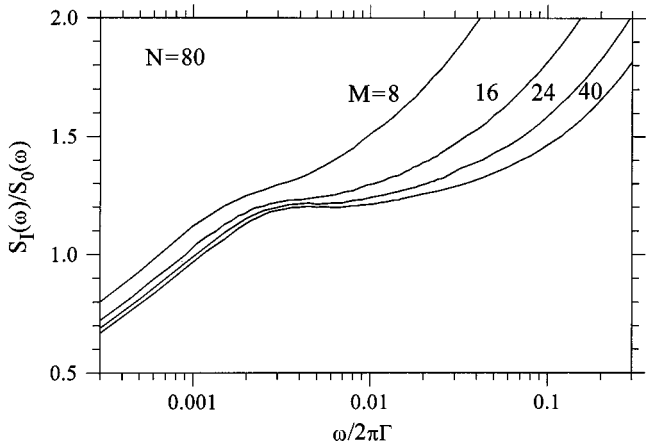

FIG. 4. Current spectral density for the array in a circle normalized by $S_0(\omega)=2eI(\omega/2\pi)^{-1/3}N^{-1}[\rho(1-\rho)]^{2/3}$ [see Eq. (21)].

$$\frac{S_I(\omega)}{2e\langle I\rangle}\simeq C\frac{(\omega/2\pi\Gamma)^{-1/3}}{N}[\rho(1-\rho)]^{2/3}, \tag{21}$$

where the numerical factor C can be found by comparison with the Monte Carlo results (Figs. 3 and 4), giving a value between 1.1 and 1.2.

Notice that Eq. (21) is accurate only if both N and M are sufficiently large. Figure 4 shows $S_I(\omega)$ normalized by the value $2e\langle I\rangle(\omega/2\pi\Gamma)^{-1/3}N^{-1}[\rho(1-\rho)]^{2/3}$ for the array with $N=80$ and different M. Even at this value of N the plateau corresponding to Eq. (21) is not yet very wide. With decreasing M the plateau shrinks and there is a noticeable deviation from Eq. (21). Nevertheless, the numerical results presented in Fig. 4 generally confirm the analytical result.

Comparing Eq. (21) with Eq. (17) it is simple to estimate the frequency of the crossover to the high-frequency limit: $\omega_h/2\pi\sim\Gamma[\rho(1-\rho)]^2$, which coincides with the frequency scale of ''collisions'' of an electron (or a hole) with its neighbors. Notice that for long arrays ($N\gg1$) the high-frequency crossover shape does not depend on N (similarly to the linear array case–see Fig. 10).

At low frequency Eq. (21) becomes invalid when the size scale L corresponding to the frequency ω_L becomes comparable with the total array length N. This allows us to estimate the position of the low-frequency crossover: $\omega_l/2\pi\simeq\tilde{C}\Gamma[\rho(1-\rho)]^{1/2}N^{-3/2}$, where $\tilde{C}$ is a numerical factor. So, we have explained the dependence $\omega_l\propto N^{-3/2}$ seen in Fig. 3. One can also check that at this frequency the result given by Eq. (21) transforms into Eq. (18).

It is interesting to find out at which electron concentration the single-particle result $F=1/N$ becomes invalid. For $N\gg1$ and small number of electrons[26] $F\simeq(M!)^2 2^{2M-1}/(2M)!N$, so that considerable deviation from the single-particle result starts already from $M=2$ and scales as $M^{1/2}$. This reflects the fact that in 1D arrays, significant correlation of hops starts at very small concentrations because randomly drifting electrons cannot pass each other.

D. Temperature effect

In the case of finite temperature when $\Gamma^-\sim\Gamma^+$, the population of all charge configurations remain equal, so the average currents satisfy the equation

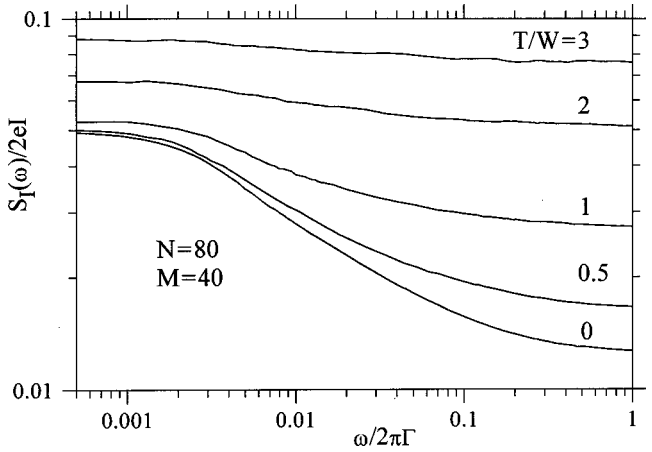

FIG. 5. Current spectral density for the ring array with $N=80$ and $M=40$ for several temperatures.

$$\langle I^{\pm}\rangle=e\Gamma^{\pm}\rho(1-\rho), \tag{22}$$

and the net current $\langle I\rangle=\langle I^+\rangle-\langle I^-\rangle$ is still given by Eq. (16) with $\Gamma=\Gamma^+-\Gamma^-$. Plugging it into Eq. (7), we get

$$S_I(\infty)/2e\langle I\rangle=\frac{1}{N}\coth(W/2T). \tag{23}$$

This result formally coincides with Eq. (13), but now it is only valid for sufficiently high frequencies.

Figure 5 shows the result of the Monte Carlo simulations for the frequency dependence of the current spectral density. As the temperature T is raised beyond the energy difference W, thermal fluctuations gradually overwhelm the correlation effects, so that the high-frequency plateau described by Eq. (23) raises and gradually ''floods'' regions of lower and lower frequencies. [The fact that the low-frequency part of the curve is less affected by thermal fluctuations can be interpreted as follows. Our arguments for Eqs. (21) and (18) were based only on equal distribution of states and Eq. (16) for the average current, which both remain unchanged for arbitrary temperature. So, as long as the temperature is small enough so that Eq. (16) is still applicable for the analysis of fluctuations at the frequency of interest, the result is virtually unchanged.] $S_I(\omega)$ may be approximately found as the largest of values given by Eq. (23) and the zero temperature result. As soon as $T\gtrsim T_c=W[N\rho(1-\rho)]^{1/2}$, the fluctuations are essentially thermal at all frequencies, and the Fano factor is given by the Nyquist expression

$$F=\frac{2T}{NW}. \tag{24}$$

Notice that as in the single-particle approximation, at $N\gg1$ there is a broad temperature region ($WN^{1/2}\ll T\ll WN$) where the array is in thermal equilibrium, while the Fano factor is still much less than 1.

E. Coulomb interaction effects

Coulomb interaction reduces the concentration fluctuations, so one could also expect a decrease of the current fluctuations. This is illustrated in Fig. 6, which shows typical Monte Carlo results for zero temperature. One can see that as

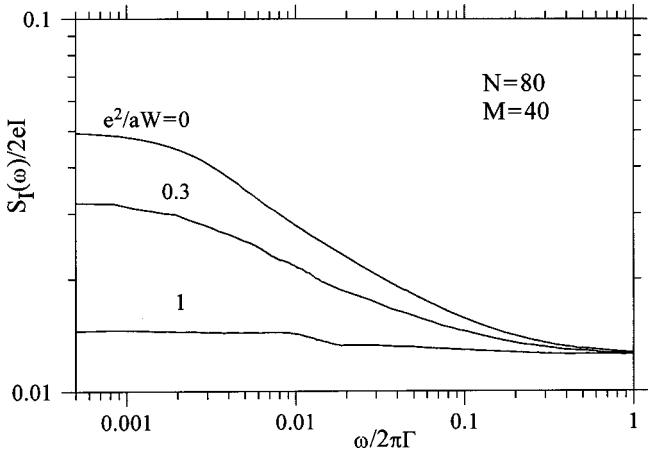

FIG. 6. Current spectral density in a ring array at zero temperature for several values of Coulomb interaction strength $r=e^2/aW$.

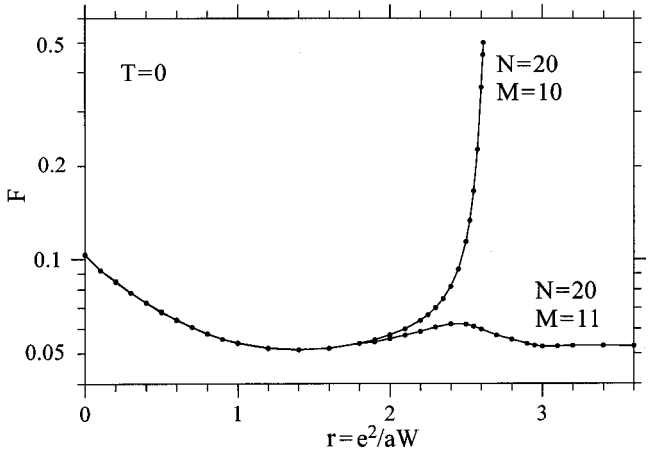

FIG. 8. The dependence of the Fano factor for the ring array on the strength r of Coulomb interaction.

soon as e^2/a becomes comparable or larger than W, the low-frequency fluctuations are gradually suppressed and can closely approach the limit (14). Figure 7 shows a typical dependence of the Fano factor on the array length N for moderate values of the relative Coulomb interaction strength $r\equiv e^2/aW$. At relatively small N the scaling $F(N)$ is in between N^{-1} and $N^{-1/2}$, while eventually at large N it reaches the dependence $F\propto N^{-1/2}$ similar to the case without Coulomb interaction. The presence of this transition is specific for 1D case, since in 1D systems the Coulomb interaction cannot provide long-range electroneutrality [because the electric field $(\rho Le)/L^2$ produced by a charged fragment of length L, decreases with L]. Hence, at large scale the density fluctuations are Coulomb decoupled, which makes the general idea of the Fano factor derivation in Sec. III C valid, leading to the scaling $F\propto N^{-1/2}$. (In contrast, in 3D case the Coulomb interaction does provide effective long-range electroneutrality, so F inversely proportional to the system size is expected.)

Stronger Coulomb interaction $(r\gtrsim[\min(\rho,1-\rho)]^{-3}/2)$ tries to fix the distance between the neighboring electrons and to turn them into a 1D Wigner crystal, which may be rotated by the external field W. The Fano factor behavior in this case may be rather complex, because it depends on whether the integers M and N are ''commensurate'' (more strictly, whether their greatest common divisor is larger than 1)—see Fig. 8. If it is, beyond some critical value r_c of the ratio e^2/aW (about 2.6 for $N=20$ and $M=10$, see Fig. 8) the Wigner crystal is stalled (at $T=0$), the system essentially turning into a Mott dielectric. At r a little less than r_c the Fano factor starts to increase rapidly from $F\gtrsim 1/N$ to some value F_c; above r_c the ratio $F=S_I(0)/2e\langle I\rangle$ is undetermined, since at $T=0$ there are neither fluctuations nor current. In the opposite case of ''incommensurate'' M and N (the greatest common divisor of M and N is 1) the Mott transition may be absent at $T=0$ even for arbitrary large r, and both the current and Fano factor may tend to the single particle results (12) and (13), respectively. It is curious that on the way to this limit the function $F(r)$ may make a bump as if it tried to mimic the behavior of its commensurate counterpart—see Fig. 8.

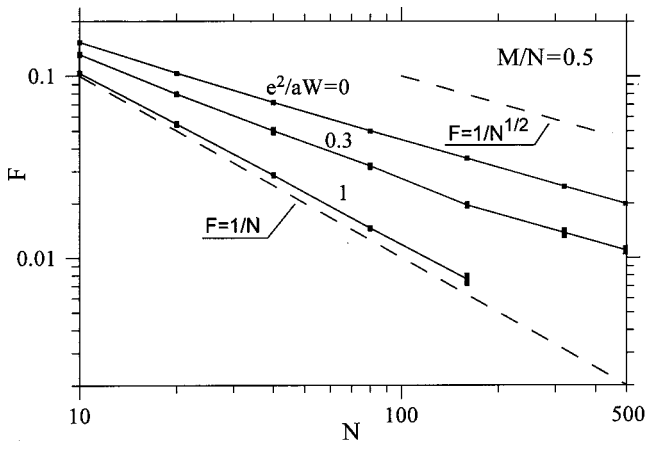

FIG. 7. Fano factor for ring arrays with a fixed electron concentration $(M/N=0.5)$ as function of the array length N, for several values of Coulomb interaction strength. Lines are just guides for the eye.

IV. LINEAR ARRAY

A. The model

The main change associated with the linear array with external electrodes [Fig. 1(a)] is that the number M of particles in the array is not more fixed. Instead, what is fixed are the chemical potentials of the metallic electrodes $\mu_{L,R}$ relative to the localized state energy. A model of the linear array should use this condition to specify rates of electron hopping between the electrodes and the edge localized sites. A reasonable way to reduce the number of additional parameters is to introduce two extra ''edge'' sites $[i=0,N$, not shown in Fig. 1(a)], which are very close to the electrodes. Then the ''edge'' tunneling rates $\Gamma^{\pm}_{L,R}$ are much higher than the ''bulk'' rates $\Gamma^{\pm}_{i}$, so that the edge sites are in thermal equilibrium with the electrodes, and the probability of their occupation may be considered fractional but fixed: $f_{L,R}=[1+\exp(-\mu_{L,R}/T)]^{-1}$. In this approximation, for a uniform array the rates of tunneling between the edge sites and their neighbors $(i=1$ and $i=N-1)$ are related to the bulk rates $\Gamma^{\pm}$ as follows:

$$\Gamma^{+}_{1}=f_L\Gamma^{+},\quad \Gamma^{+}_{N}=(1-f_R)\Gamma^{+}, \tag{25}$$

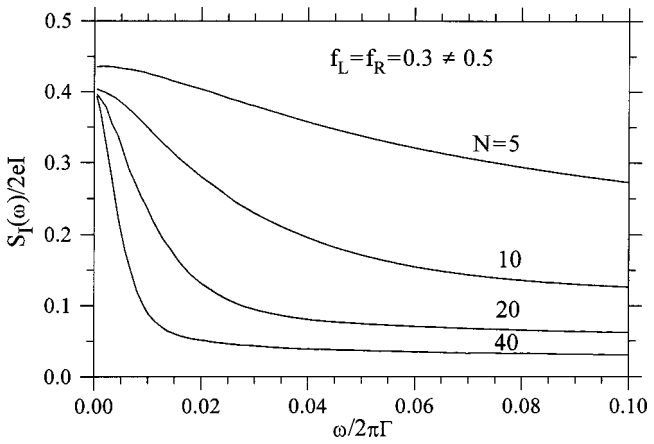

FIG. 9. Frequency dependence of the spectral density $S_I(\omega)$ for uniform linear arrays with symmetric boundary conditions, $f_L=f_R=0.3$, at $T=0$.

$$\Gamma_1^-=(1-f_L)\Gamma^-,\quad \Gamma_N^-=f_R\Gamma^+. \tag{26}$$

We will be interested in the case of identical localized sites and similar electrodes, so that $\mu_L=\mu_R$ and $f_L=f_R=f$.

External electrodes also modify the Coulomb interaction of electrons. Besides that, the image charge effect makes the self-energy of the sites dependent on their location, leading to nonuniform transport conditions. Since in the present paper we concentrate on uniform arrays, we will limit ourselves to the case of negligible Coulomb interaction.

B. Global electron number fluctuation effects

For the case of $T=0$, our model is reduced to the ASEP model with open boundaries.[26] Transport properties for the latter model have been studied in detail, especially for $f_L=f_R=f$. In this case, the probability of any charge configuration is the same[26] as if each site had independent occupation with probability f. As a consequence, the dc current is given by Eq. (16) with $\rho=f$. The Fano factor can also be calculated analytically:[27]

$$F=1-2f(1-f)\sum_{k=0}^{N-2}\frac{(2k)!}{k!(k+1)!}[f(1-f)]^k, \tag{27}$$

and for $N\to\infty$ one finds a simple result[26]

$$F=|1-2f|, \tag{28}$$

showing that the shot noise is much higher than in the circular arrays, cf., Eq. (18). Only in the evidently special point $f=1/2$, the Fano factor scales as in the closed boundary case:[27]

$$F=(\pi N)^{-1/2},\quad N\gg 1. \tag{29}$$

Figure 9 (for $f=0.3$ and several values of N) shows that $S_I(\omega)$ smoothly decreases with frequency from the value given by Eq. (28) and eventually reaches the level $S_I(\infty)=2eI/N$, in accordance with the general Eq. (7). As we will see later, at large N the frequency dependence is quite rich and exhibits three crossovers.

The fact that the low-frequency shot noise in the linear array [Fig. 1(a)] at $f\neq 1/2$ is much higher than in the ring array [Fig. 1(b)] has a simple explanation: the total number of electrons in the case of ''open boundary conditions'' may significantly fluctuate, while on the ring this number is fixed. Analytically, this effect may be especially simply considered for the case $f\ll 1$ (or similarly $1-f\ll 1$). Then the array is empty most of the time, and is entered very rarely by an electron (or hole). After the entry, the electron is transferred in a succession of hops through the array, in total transferring charge e from one electrode to another. This is exactly the situation for which the original Schottky formula was derived, so that we get $F=1$ in agreement with the corresponding limit of Eq. (28).

In the case $f\ll N^{-1/2}$ (when electrons do not collide with each other) the frequency dependence of S_I can be obtained from Eq. (14) of Ref. 38, which was derived from the orthodox theory of single-electron tunneling for the similar sequential transport scenario. Assuming that tunneling rates are equal, $\Gamma_i^+=\Gamma$, besides the negligibly small rate Γ_1^+, we get

$$\frac{S_I(\omega)}{2eI}=\frac{1}{N}+\frac{2}{N^2}\frac{\Gamma^2}{\omega^2}\left[1-\frac{\mathrm{Re}(1-\imath\omega/\Gamma)^{N-1}}{(1+\omega^2/\Gamma^2)^{N-1}}\right]; \tag{30}$$

we have confirmed this result using Monte Carlo simulations. For $N\gg 1$ this formula is reduced to

$$\frac{S_I(\omega)}{2eI}=\left[\frac{\sin(N\omega/2\Gamma)}{N\omega/2\Gamma}\right]^2, \tag{31}$$

that is obviously the normalized and squared Fourier image of the rectangular envelope of the train of N current pulses during the single-electron passage.

For $f\sim 1$, Eq. (28) may be interpreted as follows. Let us again apply Eq. (16) to long-range fluctuations. Then since $\partial I/\partial\rho=e\Gamma(1-2\rho)$, one finds $S_I(0)=e^2\Gamma^2(1-2\rho)^2S_\rho(0)$, where $S_\rho(0)$ is the low-frequency intensity of fluctuations of the total array occupation ($\rho\equiv M/N$). Notice that for $\rho=f=1/2$ the result vanishes, and we should go after the higher-order effect as we did for the ring array. For all other values of f, we may use the estimate $S_\rho(0)\sim\langle(\delta\rho)^2\rangle/\Delta\omega$, where $\langle(\delta\rho)^2\rangle=f(1-f)/N$ and the effective bandwidth $\Delta\omega$ can be estimated as $|v_s|/N$ [unlike in the ring array, the density fluctuation is carried out of the linear array with velocity v_s given by Eq. (19)]. Combining these formulas, we obtain $\Delta\omega\sim|1-2f|\Gamma/N$, $S_\rho(0)\sim f(1-f)/\Gamma|1-2f|$, and $F=\mathrm{const}\times|1-2f|$. The numerical factor in this result for the Fano factor cannot be derived in this crude way, but it obviously equals unity because at $f=1$ we should get the previous result, $F=1$. Thus we completely recover the exact result (28).

One more possible derivation of that equation can be obtained along the following line. If $f<1/2$, then the electrons can be supplied from the left electrode with the maximum rate $f\Gamma$, while the average ''sink'' velocity $(1-f)\Gamma$ is larger. Hence, only electrons relatively close to the left boundary can affect the entrance of the next electrons, and so the low-frequency correlation is essentially the boundary effect. Using this idea and taking into account, for example, correlations only due to the three first jumps, it is easy to obtain $F=1-2f+\mathcal{O}(f^3)$. Taking into account more jumps we would eventually show that Eq. (28) is exact.

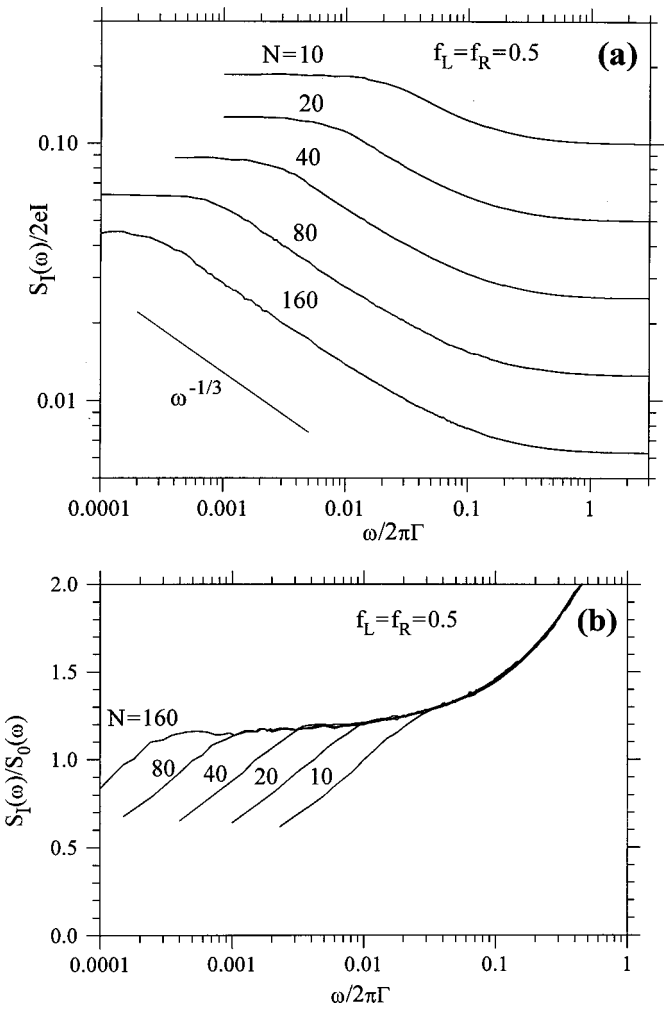

FIG. 10. (a) Current spectral density for linear array with $f_L=f_R=0.5$ at $T=0$. Notice the dependence $S_I(\omega)\sim\omega^{-1/3}$ in the intermediate frequency range between the saturations at low frequency ($F\sim N^{-1/2}$) and high frequency ($S_I(\infty)/2eI=1/N$). (b) The same data normalized by $S_0(\omega)=2eI(\omega/2\pi)^{-1/3}N^{-1}[f(1-f)]^{2/3}$.

A concentration fluctuation supplied from the boundary moves with velocity v_s, so for $N\gg 1$ the corresponding envelope in $I(t)$ has rectangular shape with duration $N/|v_s|$. Combining the corresponding frequency dependence of $S_I(\omega)$ with the exact result for F, we get

$$\frac{S_I(\omega)}{2eI}\simeq|1-2f|\left[\frac{\sin(N\omega/2\Gamma|1-2f|)}{N\omega/2\Gamma|1-2f|}\right]^2. \qquad (32)$$

At sufficiently high frequency, $\omega\gg|v_s|/N$, the ''nonlinear'' contribution from the concentration fluctuations obviously should be the same in the linear and ring arrays (with equal average concentration $\rho=f$). Hence, $S_I(\omega)$ will still be given by Eq. (21) while in the crossover region it can be crudely estimated as a sum (or maximum value) of two contributions given by Eqs. (32) and (21). As a result, there are three characteristic frequencies in $S_I(\omega)$ dependence at $N\gg 1$: the low-frequency saturation occurs at $\omega\lesssim\omega_l\sim\Gamma|1-2f|/N$, the intermediate-frequency dependence described by Eq. (21) starts at $\omega\gtrsim\omega_m\sim\Gamma N^{-3/5}|1-2f|^{9/5}[f(1-f)]^{-2/5}$, and finally the high-frequency saturation occurs at $\omega\gtrsim\omega_h\sim\Gamma[f(1-f)]^2$, similar to the ring array case.

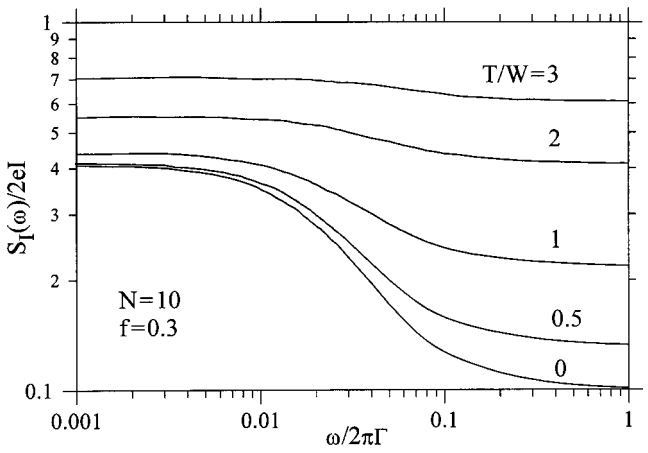

FIG. 11. Frequency dependence of the current spectral density in the linear array with $N=10$ and $f_L=f_R=0.3$ at several temperatures.

The case $f=1/2$ plays a special role in the ASEP theory, as can be easily noticed comparing Eqs. (28) and (29). Actually, this case is quite important since for sufficiently long arrays with $f_L>1/2$ and $f_R<1/2$ the electron concentration in the bulk of the array is close[26] to $f=1/2$ (so $\langle I\rangle=e\Gamma/4$) and, hence, the scaling $F\propto N^{-1/2}$ holds as in Eq. (29). [As an example, for $f_L=1$, $f_R=0$ the result is[27] $F=3(2\pi)^{1/2}/16N^{1/2}$.] At $f=1/2$ the low-frequency fluctuations can no longer be considered as a boundary effect, since the ''sink'' velocity $(1-f)\Gamma$ is equal in this case to the maximum supply rate $f\Gamma$; hence, the transport becomes jammed and the correlations involve the whole array length.

In the respect that the boundary effects are no longer important, the linear array at $f=1/2$ is very similar to the circle array. Figure 10 shows the frequency dependence of the current spectral density for $f=1/2$ and several values of N. The data look similar to that in Fig. 3. The main feature is $\omega^{-1/3}$ dependence in the intermediate frequency range. To check the validity of Eq. (21) in this range, Fig. 10(b) shows the same data as Fig. 10(a) but normalized by $S_0(\omega)=2eI(\omega/2\pi)^{-1/3}N^{-1}[f(1-f)]^{2/3}$. We see that as N grows, the intermediate region becomes more and more pronounced.

C. Temperature effects

Figure 11 shows the numerically calculated effect of nonvanishing temperature on the shot noise in a linear array. It shows that the effect is quite similar to that in a ring array (Fig. 5), however, because of the higher initial intensity of low-frequency fluctuations (at $T=0$) the noise becomes completely thermal at a higher temperature, $T\gtrsim W|1-2f|$.

V. DISCUSSION

Probably the most important result of our analysis is that in contrast to the expectation based on the analysis of 1D arrays of conventional tunnel junctions, the shot noise in uniform 1D hopping arrays is typically much higher than $1/N$ of the Schottky value $S_I=2e\langle I\rangle$. However, in some

cases this lower bound can be achieved. In order to sort out these cases, it is useful to consider the current fluctuations as the result of three major sources:

- time randomness of electron tunneling events,
- electron density fluctuations, and
- thermal fluctuations.

Crudely speaking, the lower bound $2e\langle I\rangle/N$ for the noise is determined by the first contribution, while the second contribution typically increases the noise significantly even at $T=0$.

At relatively high frequencies the current spectral density in a ring array and 1D array between electrodes behaves pretty similarly. In particular, the high-frequency asymptote is given by the same Eq. (7) and is determined by capacitive factors λ_i. (This result is also valid for the conventional case of 1D array of tunnel junctions–see Appendix). If $\lambda_i=1/N$, then in all cases at low temperature T we have $S_I(\infty)=2e\langle I\rangle/N$.

However, at low frequency the noise behavior in a ring array and a linear array is quite different. The reason for the difference is that in a linear array the total number of electrons can fluctuate while in the ring array it is fixed. In the case when the single-particle approximation is applicable for a linear array, the relative density fluctuations are maximal, and the Fano factor is not suppressed: $F=1$ at $T=0$. The electron ''collisions'' (the Pauli exclusion) reduce these fluctuations, but quite inefficiently. Only in the special case of half-filling ($f=0.5$) when ''traffic jams'' have all size scales, the Fano factor decreases as $N^{-1/2}$ with the array length N; in other cases the dependence $F(N)$ quickly saturates at the level $F=|1-2f|$. One can speculate that Coulomb interaction should be a more efficient factor in suppression of F, since it may significantly reduce the electron density fluctuations, however, this conclusion has still to be verified numerically.

In contrast to the linear array, in the uniform ring array the uncorrelated motion (of a single electron) provides the maximal suppression of the Fano factor, $F=1/N$. The Pauli exclusion in fact increases F leading to $F\propto N^{-1/2}$. However, the extra correlations due to Coulomb interaction between electrons on different sites make transport ''smoother'' and reduce the Fano factor, in some cases down to the lower bound $F=1/N$.

It is instructive to compare these results with those for a 1D array of tunnel junctions (see Appendix). In the latter model the Fano factor is determined purely by the junction resistances. In some sense, this is a consequence of strong Coulomb interaction that forbids noticeable charge fluctuations and establishes fast long-range correlations between currents through different tunnel junctions. In the uniform array at low temperature the noise suppression is maximal, $F=1/N$. However, if the junctions are very small, single-electron effects can lead to significant charge fluctuations and thus increase the Fano factor. For example, $F=1$ is realized[4] in the vicinity of the Coulomb blockade threshold when the transport has a bottleneck even in the uniform array.

So far we have reviewed our results for the uniform case. Now let us briefly discuss hopping transport noise in nonuniform 1D arrays. It is simple to study one particle inside the ring array with arbitrary disorder at low temperatures. In this case the transport is unidirectional, $\Gamma_i^-=0$, and the average current is obviously given by the expression

$$\langle I\rangle = e\left[\sum_i (\Gamma_i^+)^{-1}\right]^{-1}, \tag{33}$$

while the formula for the current spectral density has been derived in Ref. 38 for the case $\lambda_i=1/N$, and can be readily generalized to include arbitrary λ_i:

$$S_I(\omega)=2e\langle I\rangle\sum_{l=1}^{N}\lambda_l^2+4e\langle I\rangle\mathrm{Re}\left\{\left[\prod_{l=1}^{N}\left(1+\frac{\imath\omega}{\Gamma_l^+}\right)-1\right]^{-1}\times\left[\sum_{l=1}^{N}\lambda_l^2+\sum_{l=1}^{N-1}\sum_{m=1}^{N}\lambda_m\lambda_{m+l}\prod_{k=1}^{l}\times\left(1+\frac{\imath\omega}{\Gamma_{k+m}^+}\right)\right]\right\}, \tag{34}$$

where by definition $\Gamma_{N+k}^+=\Gamma_k^+$. At zero frequency this formula is reduced to

$$\frac{S_I(0)}{2e\langle I\rangle}=\left[\sum_i (\Gamma_i^+)^{-2}\right]\left[\sum_i (\Gamma_i^+)^{-1}\right]^{-2}, \tag{35}$$

and allows us to study the statistics of the Fano factor for random distribution of Γ_i^+ in a long array, $N\gg 1$.

As the major factor, let us take into account the dependence of tunneling rate on the distance a_i between sites, $\Gamma_i^+=\Gamma_0\exp(-2a_i/\xi)$, where ξ is the localization length, and assume that independent random a_i obey the Poisson distribution, $p(a_i)=a_0^{-1}\exp(-a_i/a_0)$ where $a_0\gg\xi$ is the average spacing. Then the distribution of rates can be parameterized as $\Gamma_i^+=\Gamma_0 x_i^{2a_0/\xi}$, where the random number x_i has uniform distribution between 0 and 1. The minimal rate (''bottleneck'') Γ_{min} will be about $\Gamma_0(2a_0/\xi\mathrm{e}N)^{2a_0/\xi}$ on average (here $\mathrm{e}=2.71$), while the next minimal rate Γ_{min+1} will be much larger, $\Gamma_{min+1}/\Gamma_{min}\sim(2a_0/\xi\mathrm{e}N)^{-2a_0/\xi}\gg 1$. It is easy to see that in this case both the average current [Eq. (33)] and the Fano factor [Eq. (35)] are determined by the bottleneck: $\langle I\rangle=e\Gamma_{min}$ and $F=1$.

It is also instructive to consider a model where the maximal distance a_i is limited by some big value a_{max} ($a_{max}\gg a_0$). For example, this describes the situation in which some other transport mechanism starts to dominate over tunneling when the sites are too far apart, thus limiting Γ from below. If $N\ll\exp(a_{max}/a_0)$, the results for the average current and the Fano factor do not differ from the case considered above. However, for very long arrays, $N\gg\exp(a_{max}/a_0)$, the transport is limited by many similar bottlenecks, so that $\langle I\rangle\simeq e\Gamma_0\exp(-2a_{max}/\xi+a_{max}/a_0)/N$ and the Fano factor decreases with the array length, $F\simeq\exp(a_{max}/a_0)/N$.

We can use this result for a preliminary estimate of the Fano factor for hopping in disordered 2D and 3D systems when the transport is mainly determined by percolation clusters.[21] If the single-particle approach is applicable, then as in the case above we can simply count the number of similar bottlenecks in the transport direction. With this argument, we obtain a simple estimate

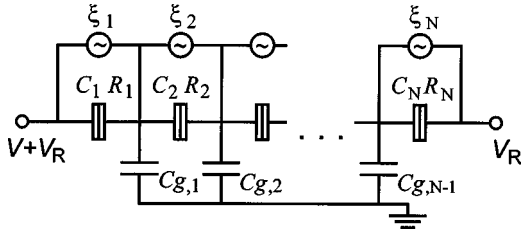

FIG. 12. 1D array of N tunnel junctions with capacitances C_i and resistances R_i, while $C_{g,i}$ are the capacitances to the ground. The Langevin noise sources are presented by random current generators $\xi_i(t)$ parallel to the junctions.

$$F \sim L_c/L, \tag{36}$$

where L is the sample length and L_c is the characteristic size of the percolation cluster. The applicability range of the approach is rather unclear, so this result still has to be confirmed using either more quantitative analysis or numerical Monte Carlo modeling. (Preliminary numerical analysis of 2D hopping on uniform slanted square lattice gives the dependence[39] $F \propto L^{-\nu}$ where $\nu \simeq 0.85$ is rather close but different from unity.)

In conclusion, in the present paper we have studied the shot noise at hopping in 1D arrays of sites, concentrating on the uniform case and briefly considering the effect of disorder. It is important to extend this study to 2D and 3D hopping. The presented results hint that the Coulomb interaction may play the crucial role in the suppression of low-frequency shot noise.

ACKNOWLEDGMENTS

Fruitful discussions with D. A. Parshin and V. V. Kuznetsov are gratefully acknowledged. This work was supported in part by the Engineering Research Program of the Office of Basic Energy Sciences at the Department of Energy.

APPENDIX: 1D ARRAY OF TUNNEL JUNCTIONS

In this Appendix we calculate the spectral density of the shot noise in a 1D array of tunnel junctions. We will first use the standard circuit theory and then extend the calculations to the case of weak single-electron effects (which are assumed to be small because of high temperature or high current).

Figure 12 shows the array of N tunnel junctions in series. Each junction is characterized by resistance R_i and capacitance C_i ($i=1,\ldots,N$), while $C_{g,k}$ ($k=1,\ldots,N-1$) denote capacitances of ''islands'' to the ground. This circuit does not describe the long-range capacitances which can be especially important for islands and junctions of small size,[40] that can require numerical calculation of the total capacitance matrix.[40–42] The derivation below is valid for arbitrary capacitance matrix, however, for simplicity we will refer to Fig. 12.

In the absence of single-electron correlations the I-V curve of the array is linear, $\langle I\rangle = V/R_\Sigma$, $R_\Sigma = \Sigma_i R_i$, and the average voltage across each junction is proportional to the junction resistance, $\langle V_i\rangle = \langle I\rangle R_i$. To study the fluctuations we follow the standard circuit theory[22] and introduce the sources of the current noise $\xi_i(t)$ in parallel with the junctions. Separating the current through ith junction into two parts flowing in opposite directions,

$$\langle I\rangle = \langle I_i^+\rangle - \langle I_i^-\rangle, \quad \langle I_i^+\rangle/\langle I_i^-\rangle = \exp(-e\langle V_i\rangle/T), \tag{A1}$$

and using the Schottky formula for each part, we get the following white $[S(\omega)=S(0)]$ spectral density for the noise source $\xi_i(t)$:

$$S_{\xi i}(\omega) = 2e\langle I_i^+\rangle + 2e\langle I_i^-\rangle = 2e\langle I\rangle \coth(e\langle V_i\rangle/2T). \tag{A2}$$

Let us denote by $\phi_i(t)$ the fluctuating part of the ith island potential [$\phi_0(t)=\phi_N(t)=0$ because we assume constant potentials of the leads], then the current $I_i(t)$ through ith junction can be written as

$$I_i(t) = \langle I\rangle + [\phi_{i-1}(t) - \phi_i(t)]/R_i + \xi_i(t). \tag{A3}$$

The evolution of $\phi_i(t)$ is described by the equation

$$\dot{\phi}_i = \sum_{j=1}^{N} I_k(t)[D_{i,j} - D_{i,j-1}], \tag{A4}$$

where $\mathbf{D} \equiv \mathbf{C}^{-1}$ is the inverse capacitance matrix (obviously $D_{i,j}=D_{j,i}$ and $D_{0,i}=D_{N,i}=0$) and can be rewritten in the following form:

$$\dot{\phi}_i = \sum_{k=1}^{N-1} A_{i,k}\phi_k + \sum_{k=1}^{N} B_{i,k}\xi_k, \tag{A5}$$

$$A_{i,k} \equiv B_{i,k+1}/R_{k+1} - B_{i,k}/R_k, \tag{A6}$$

$$B_{i,k} \equiv D_{i,k} - D_{i,k-1}. \tag{A7}$$

Notice that $\mathbf{A}$ is $(N-1)\times(N-1)$ matrix while $\mathbf{B}$ is $(N-1)\times N$ matrix. In the frequency representation Eq. (A5) can be written as $\imath\omega\boldsymbol{\phi}(\omega) = \mathbf{A}\phi(\omega) + \mathbf{B}\xi(\omega)$ ($\imath$ is the imaginary unit) and can be easily solved in the matrix form,

$$\phi(\omega) = \left(\frac{\mathbf{1}}{\imath\omega\mathbf{1} - \mathbf{A}}\right)\mathbf{B}\xi(\omega). \tag{A8}$$

Using Eq. (A3) we find the Fourier transform of $I_i(t)$:

$$I_i(\omega) = \sum_{j=1}^{N} X_{i,j}(\omega)\xi_j(\omega), \tag{A9}$$

$$X_{i,j}(\omega) = \delta_{ij} + \frac{1}{R_i}\sum_{k=1}^{N-1}\left[\left(\frac{1}{\imath\omega - \mathbf{A}}\right)_{i-1,k} - \left(\frac{1}{\imath\omega - \mathbf{A}}\right)_{i,k}\right]B_{k,j}, \tag{A10}$$

where by definition $(\imath\omega - \mathbf{A})^{-1}_{0,k} = (\imath\omega - \mathbf{A})^{-1}_{N,k} = 0$.

Notice that at $\omega \to \infty$ the only surviving term in Eq. (A10) is the Kronecker symbol δ_{ij} so that

$$I_i(\infty) = \xi_i(\infty). \tag{A11}$$

At $\omega = 0$ it is possible to prove (using somewhat cumbersome algebra) the relation

$$I_i(0) = \sum_j (R_j/R_\Sigma)\xi_j(0), \tag{A12}$$

which obviously means that at low frequencies the current is distributed according to resistances and equal in all junctions. [Equation (A12) shows that the fraction R_j/R_Σ of the current ξ_j flows through the array while the rest is returned via the ''shunt'' R_j.]

The spectral density of the current I_i through ith junction can be readily calculated as

$$S_{Ii}(\omega)=\sum_j |X_{i,j}(\omega)|^2 S_{\xi j}, \tag{A13}$$

because the noise sources ξ_j are mutually uncorrelated [since $S_{\xi j}(\omega)$ does not depend on frequency, we omit ω]. Using Eqs. (A2), (A11), and (A12) we get the simple expressions in the limiting cases:

$$S_{Ii}(0)=2e\langle I\rangle\sum_j (R_j^2/R_\Sigma^2)\coth(e\langle I\rangle R_j/2T), \tag{A14}$$

$$S_{Ii}(\infty)=2e\langle I\rangle\coth(e\langle I\rangle R_i/2T). \tag{A15}$$

In experiment it is usually impossible to measure the current through one junction, and the only measurable quantity is the current in the external lead, which contains the contribution from the displacement current and, hence, depends on the currents through all junctions. The current $I(t)$ at the left external lead can be expressed as the linear combination,

$$I(t)=\sum_i \lambda_i I_i(t), \tag{A16}$$

$$\lambda_i=\delta_{1i}+\sum_j C_{0,j}B_{j,i}, \quad \sum_i \lambda_i=1, \tag{A17}$$

where $C_{0,k}$ is the element (always negative) of the capacitance matrix between the left electrode and kth island. In the case of Fig. 12, $C_{0,k}=-C_1\delta_{1k}$ because the left electrode is capacitively coupled only with the first island, so $\lambda_i=\delta_{1i}-C_1B_{1,i}$. If all $C_{g,i}=0$ in Fig. 12, then $\lambda_i=C_i^{-1}/\Sigma_j C_j^{-1}$, while for a long uniform array, $C_i=C=\text{const}$, $C_{g,i}=C_g=\text{const}$, $N^2\gg C/C_g$, the coefficients are $\lambda_i=\mathcal{X}^{i-1}(1-\mathcal{X})$, where $\mathcal{X}=1+C_g/2C-[(C_g/2C)^2+C_g/C]^{1/2}$. If the tunneling system is different from what is shown in Fig. 12 and consists of small islands which are separated by much larger distances and imbedded into the plane capacitor (external electrodes), then similar to the hopping case $\lambda_i=a_i/\Sigma_j a_j$, where a_i is the length of the projection of ith tunneling jump onto the direction perpendicular to the capacitor planes.

Using Eqs. (A16) and (A9) we obtain the following expression for the spectral density of the left external current:

$$S_I(\omega)=\sum_j \left|\sum_i \lambda_i X_{i,j}(\omega)\right|^2 S_{\xi j} \tag{A18}$$

[notice that at finite frequency, $S_I(\omega)$ for the left and right electrodes can be different]. In the particular case shown in Fig. 12,

$$\sum_i \lambda_i X_{i,j}=\delta_{1j}-C_1B_{1,j}-\sum_{m,k}^{N-1}\left[\frac{\delta_{1m}}{R_1}+C_1A_{1,m}\right]\times\left(\frac{1}{\imath\omega-\mathbf{A}}\right)_{m,k}B_{k,j}. \tag{A19}$$

In the limit $\omega=0$ the spectral density $S_I(0)$ of the external current coincides with the spectral density of the current through any junction (see Sec. II) and, hence, is given by Eq. (A14). While at low-frequency S_I is determined only by the circuit resistances, in the opposite limit, $\omega\to\infty$, it is determined mainly by the circuit capacitances,

$$S_I(\infty)=\sum_i \lambda_i^2 S_{\xi i}=2e\langle I\rangle\sum_i \lambda_i^2\coth(e\langle I\rangle R_i/2T) \tag{A20}$$

(resistances are important only when the Nyquist noise contribution is considerable, $T\gtrsim IR_i$). It is simple to check that in the thermal equilibrium, $I=0$, the low-frequency noise [see Eq. (A14)] always satisfies the Nyquist formula, $S_I(0)=4T/R_\Sigma$, however, at finite frequency the noise is different for example, $S_I(\infty)=4T\Sigma_i\lambda_i^2/R_i$. Notice that in this formalism $\omega=\infty$ still means $\hbar\omega\ll\max(T,eV_i)$. However, it would be simple to take into account zero-point fluctuations by replacing Eq. (A2) with[43] $S_{\xi i}(\omega)=R_i^{-1}\Sigma_\pm(eV_i\pm\hbar\omega)\coth[(eV_i\pm\hbar\omega)/2T]$.

In a uniform array at zero temperature the noise at low frequency is suppressed N times [see Eq. (A14)] in comparison with the Schottky formula, $S_I(0)=S_{Ii}(0)=2eI/N$. However, at high frequency the suppression of the external current noise is usually weaker, $S_I(\infty)=2eI\Sigma_i\lambda_i^2$, $1/N\leqslant\Sigma_i\lambda_i^2\leqslant 1$, while for the current through a particular junction there is no suppression at all, $S_{Ii}(\infty)=2eI$.

It is interesting to find out at which ω the low-frequency result is no longer accurate. We have studied the long uniform arrays shown in Fig. 12, $N\gg(C/C_g)^{1/2}$, and found numerically that the relative accuracy $\epsilon\ll 1$ of the low-frequency result, $S_I(\omega)/2eI=(1+\epsilon)/N$, corresponds to the frequency $\omega/2\pi\simeq 1.1(RC_g)^{-1}\epsilon^{1/2}N^{-2}$. This formula, however, cannot be used to describe the crossover to the high-frequency asymptote, $S_I(\infty)=(1+4C/C_g)^{-1/2}$.

If the typical size of the tunnel junctions is small, single-electron effects[29] become important. Below we extend the standard noise theory to this case, assuming that single-electron effects are weak due to relatively high temperature, $T\gtrsim e^2/\tilde{C}$, or relatively high current, $I\gtrsim e/\tilde{R}\tilde{C}$ ($\tilde{C}$ and $\tilde{R}\gg R_Q$ are the typical capacitance and resistance of tunnel junctions).

According to the ''orthodox'' theory,[29] the rate of tunneling through ith junction (in the positive direction),

$$\Gamma=V_i^{eff}/eR_i[1-\exp(-eV_i^{eff}/T)] \tag{A21}$$

is governed by the effective voltage V_i^{eff}, which is always smaller than the actual voltage V_i,

$$V_i^{eff}=V_i-e/2C_{t,i}, \tag{A22}$$

$$1/C_{t,i}=D_{i-1,i-1}+D_{i,i}-2D_{i-1,i}, \tag{A23}$$

where $C_{t,i}$ is the total capacitance of ith junction. (For tunneling in the opposite direction the effective voltage is $-V_i - e/2C_{t,i}$.) Linearizing Eq. (A21) and averaging over the fluctuating $V_i(t)$, we obtain the equation

$$\langle I\rangle = \langle I_i^+\rangle - \langle I_i^-\rangle, \tag{A24}$$

$$\langle I_i^{\pm}\rangle = \frac{\pm\langle V_i\rangle - e/2C_{t,i}}{R_i[1-\exp(-e(\pm\langle V_i\rangle - e/2C_{t,i})/T)]}, \tag{A25}$$

which allows us to calculate the average voltages $\langle V_i\rangle$ for the given average current $\langle I\rangle$. (Notice that the high-voltage offset of the I-V curve is equal to $V_{off}=\Sigma_i e/2C_{t,i}$ exactly.) This approximation has been successfully used for the analytical and numerical analysis of the I-V curves of Coulomb blockade thermometers.[44]

Since we assumed an essentially linear response of any junction current, it is natural to use the formalism of the standard circuit theory, so the result for the current spectral density will be given by the same Eqs. (A10), (A13), and (A17)–(A19). However, the second equality in Eq. (A2) is no longer valid, and we have at least three reasonable choices for the ''seed'' noise spectral density: $S_{\xi i}=2e\langle I_i^+\rangle+2e\langle I_i^-\rangle$, $S_{\xi i}=2e\langle I\rangle\coth(e\langle V_i\rangle/2T)$, or $S_{\xi i}=2e\langle I\rangle\coth(e\langle I\rangle R_i/2T)$. The first choice seems to be the most natural one, however, numerical comparison with the results of Monte Carlo simulations shows that the first formula usually underestimates noise (see Fig. 13), the third formula overestimates it, and the second formula (which is in between two others) usually gives the closest result, though not always. Notice, however, that all three approximations coincide in the limits of both low and high temperature, so the difference between them is never too significant within the applicability range of the formalism.

As the next level of approximation for the ''seed'' noise $S_{\xi i}$ at finite temperature, it is possible to estimate the standard deviation of fluctuating $V_i(t)$ and take into account the correction due to the second derivative of Eq. (A21). It is also possible to take into account the effective increase of the junction resistances used in the evolution equation (A3) at finite temperatures (we did not implement this last idea numerically). Figure 13 shows the frequency dependence of the spectral density of the current in the (left) external electrode for the uniform array of $N=10$ junctions with $C_g/C=0.1$ symmetrically biased by voltage $V=5e/C$ at temperature $T=e^2/C$. The thick line shows the results of Monte Carlo simulations while the thin lines represent the calculations using Eqs. (A18)–(A19). For the lowest and highest thin lines, the first and third formulas for $S_{\xi i}$ discussed above have been used. The thin line corresponding to the second formula is almost indistinguishable from the thin line showing the result using the second (quadratic) approximation of $S_{\xi i}$. As one can see, these lines are quite close to the Monte Carlo result. With an increase of current or temperature all thin lines become closer to each other, and the agreement with the Monte Carlo result becomes even better.

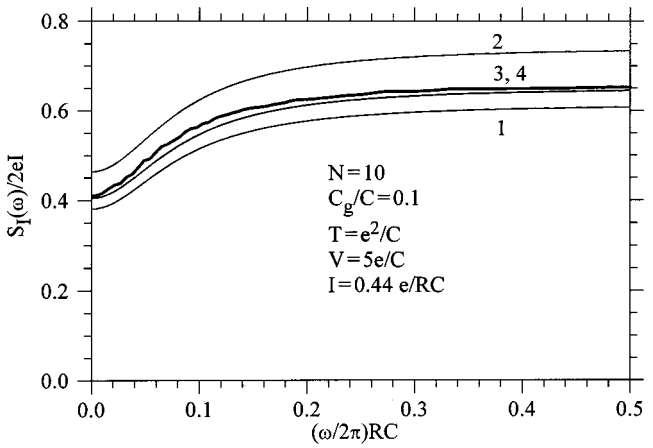

FIG. 13. Normalized spectral density $S_I(\omega)$ for a uniform array of small tunnel junctions. Thick line shows the result of Monte Carlo simulations while thin lines 1–4 are calculated using Eqs. (A18)–(A19). For lines 1–3 the ''seed'' noise $S_{\xi i}$ is calculated as $2e(\langle I_i^+\rangle+\langle I_i^-\rangle)$, $2e\langle I\rangle\coth(e\langle I\rangle R_i/2T)$, and $2e\langle I\rangle\coth(e\langle V_i\rangle/2T)$, respectively. For the line 4 (by coincidence, almost indistinguishable from line 3) $S_{\xi i}$ is calculated using the quadratic approximation.

[1] Sh. Kogan, *Electronic Noise and Fluctuations in Solids* (Cambridge University Press, Cambridge, 1996).

[2] M.J.M. de Jong and C.W.J. Beenakker, in *Mesoscopic Electron Transport*, edited by L.L. Sohn, L.P. Kouwenhoven, and G. Schön, NATO ASI Vol. 345 (Kluwer, Dordrecht, 1997), p. 225.

[3] Ya.M. Blanter and M. Buttiker, e-print cond-mat/9910158.

[4] K.A. Matsuoka and K.K. Likharev, Phys. Rev. B **57**, 15 613 (1998).

[5] K. Likharev, Proc. IEEE **87**, 606 (1999).

[6] A. Korotkov, Int. J. Electron. **86**, 511 (1999).

[7] G.B. Lesovik, Pis'ma Zh. Éksp. Fiz. **49**, 513 (1989) [JETP Lett. **49**, 592 (1989)].

[8] Th. Martin and R. Landauer, Phys. Rev. B **45**, 1742 (1992).

[9] Y. Naveh, A.N. Korotkov, and K.K. Likharev, Phys. Rev. B **60**, R2169 (1999).

[10] K.E. Nagaev, Phys. Lett. A **169**, 103 (1992).

[11] C.W.J. Beenakker and M Büttiker, Phys. Rev. B **46**, 1889 (1992).

[12] K.E. Nagaev, Phys. Rev. B **52**, 4740 (1995).

[13] Y. Naveh, D.V. Averin, and K.K. Likharev, Phys. Rev. Lett. **79**, 3482 (1997).

[14] Y. Naveh, D.V. Averin, and K.K. Likharev, Phys. Rev. B **58**, 15 371 (1998); **59**, 2848 (1999).

[15] A.N. Korotkov, D.V. Averin, K.K. Likharev, and S.A. Vasenko, in *Single-Electron Tunneling and Mesoscopic Devices*, edited by H. Koch and H. Lübbig (Springer, Berlin 1992), p. 45.

[16] A.N. Korotkov, Phys. Rev. B **49**, 10 381 (1994).

[17] S. Hershfield, J.H. Davies, P. Hyldgaard, C.J. Stanton, and J.W. Wilkins, Phys. Rev. B **47**, 1967 (1993).

[18] U. Hanke, Yu. M. Galperin, K.A. Chao, and N. Zou, Phys. Rev. B **48**, 17 209 (1993).

[19] W. Zheng, J.R. Friedman, D.V. Averin, S.Y. Han, and J.E. Lukens, Solid State Commun. **108**, 839 (1998).

[20] N.F. Mott and E.A. Davis, *Electronic Processes in Non-Crystalline Materials*, 2nd ed. (Clarendon Press, Oxford, 1979).

[21] B.I. Shklovskii and A.L. Efros, *Electronic Properties of Doped Semiconductors* (Springer, Berlin, 1984).
[22] A. van der Ziel, *Noise* (Prentice-Hall, New York, 1954).
[23] R. Landauer, Physica B **227**, 156 (1996).
[24] Sh. Kogan, Phys. Rev. B **57**, 9736 (1998).
[25] There have been, however, several noise analyses (Refs. 26–28), which are partly relevant for our work goals; we will refer to them at appropriate occasions below.
[26] B. Derrida, Phys. Rep. **301**, 65 (1998).
[27] B. Derrida, M.R. Evans, and K. Mallick, J. Stat. Phys. **79**, 833 (1995).
[28] H.J. Jensen, Phys. Rev. Lett. **64**, 3103 (1990).
[29] D.V. Averin and K.K. Likharev, in *Mesoscopic Phenomena in Solids*, edited by B. Altshuler *et al.* (Elsevier, Amsterdam, 1991), Chap. 6.
[30] A.N. Korotkov, Europhys. Lett. **43**, 343 (1998).
[31] K.K. Likharev, N.S. Bakhvalov, G.S. Kazacha, and S.I. Serduykova, IEEE Trans. Magn. **25**, 1436 (1989).
[32] The quantum coherence can be neglected, for example, if the dephasing due to interaction with phonons is faster than the frequency of Rabi oscillations between neighboring sites.
[33] W is sometimes called the electrochemical potential difference of neighboring sites (see, e.g., Ref. 34). However, since in the standard definition of the electric potential the charge is assumed to be continuous, one should be careful to apply this terminology to systems with discrete charge (Ref. 29).
[34] L.P. Kouwenhoven, C.M. Marcus, P.L. McEuen, S. Tarucha, R.M. Westervelt, and N.S. Wingreen, in *Mesoscopic Electron Transport* (Ref. 2), p. 105.
[35] The results are also valid at $M=N-1$, when only one hole is present in the array. Similar results would be also valid in the case of an arbitrary number of electrons, if they were not correlated either due to the Pauli principle (imbedded into our model) or Coulomb interaction.
[36] The self-organized criticality has been shown (Ref. 28) to lead to $1/f$ power spectrum in a somewhat different model describing the flux flow in superconductors.
[37] S.M. Rytov, Yu.A. Kravtsov, and V.I. Tatarskii, *Principles of Statistical Radiophysics*, Vol. 2 (Springer, Berlin, 1988).
[38] A.N. Korotkov, Phys. Rev. B **50**, 17 674 (1994).
[39] V.A. Sverdlov, Y. Kinkhabwala, A.N. Korotkov, and K.K. Likharev, Bull. Am. Phys. Soc. March Meeting 2000, Report I28 9, p. 457.
[40] K.K. Likharev and K.A. Matsuoka, Appl. Phys. Lett. **67**, 3037 (1995).
[41] A.N. Korotkov, Appl. Phys. Lett. **67**, 2412 (1995).
[42] A.N. Korotkov and K.K. Likharev, J. Appl. Phys. **84**, 6114 (1998).
[43] A.J. Dahm, A. Denenstein, D.N. Langenberg, W.H. Parker, D. Rogovin, and D.J. Scalapino, Phys. Rev. Lett. **22**, 1416 (1969).
[44] K.P. Hirvi, J.P. Kaupinen, A.N. Korotkov, M.A. Paalanen, and J.P. Pekola, Appl. Phys. Lett. **67**, 2096 (1995).